




Synthesis of β -FeOOH/Fe₃O₄ hybrid photocatalyst using catechol-quaternized poly(*N*-vinyl pyrrolidone) as a double-sided molecular tape

Nur'aeni², Ari Chae², Seongho Jo², Yujin Choi², Byoungnam Park⁴, Sung Young Park^{2,3,*}, and Insik In^{1,2,*} 

¹Department of Polymer Science and Engineering, Korea National University of Transportation, Chungju-Si 380-702, South Korea

²Department of IT Convergence (Brain Korea PLUS 21), Korea National University of Transportation, Chungju 380-702, South Korea

³Department of Chemical and Biological Engineering, Korea National University of Transportation, Chungju 380-702, South Korea

⁴Department of Materials Science and Engineering, Hongik University, Seoul 121-791, South Korea

Received: 30 December 2016

Accepted: 10 February 2017

Published online:

7 April 2017

© Springer Science+Business Media New York 2017

ABSTRACT

Mussel-inspired linking of β -FeOOH (akaganeite) on core Fe₃O₄ nanoparticles (NPs) was successfully attempted to produce a novel hybrid photocatalyst that facilitates both visible-light-driven photocatalysis and easy recovery using an external magnetic force. A catechol-quaternized poly(vinyl pyrrolidone) was adopted as a double-sided molecular tape between β -FeOOH and the Fe₃O₄ NPs, which successfully incorporated robust molecular linking. The β -FeOOH/Fe₃O₄ hybrid photocatalysts showed photodegradation efficiencies greater than 90% within 3 h of using rhodamine B as a model compound for environmental pollutants upon irradiation of visible light using a lamp through the heterogeneous photo-Fenton-like process in the presence of H₂O₂. The β -FeOOH/Fe₃O₄ hybrid photocatalyst is a promising visible-light-driven photocatalyst due to its narrow band gap 1.79 eV, and it can be repeatedly recovered and recycled up to 4 cycles. This concept of double-sided molecular tape can be widely applied for the generation of novel and robust hybrid nanomaterials, affording synergistic performance enhancements.

Introduction

Molecular linking of two different nanomaterials can induce a synergic function in everyday life; in the research field, it can help meet the increased demand for hybrid nanomaterials in various applications. It has been recently reported that adherent Mefp-5

(*Mytilus edulis* foot protein-5), a foot protein that mussels release for holding onto rocks in a sea environment, contains a large amount of catechol derivatives; hence, Mefp-5 is very promising for the molecular linking of two nanomaterials with different structural or compositional features to provide hybrid nanomaterials for many applications, including nanocomposites, solar energy harvesting, and

Address correspondence to E-mail: parkchem@ut.ac.kr; in1@ut.ac.kr

pseudocapacitors [1–4]. In particular, molecular linking through mussel-inspired chemistry is accessible for many kinds of materials or substrates, including metals, metal oxides, carbon nanomaterials, and polymers [3].

Considering the benefit of mussel-inspired chemistry, molecular linking of a photocatalyst and magnetic NPs was performed to construct magnetically recyclable visible-light-driven hybrid photocatalysts in this study. Photocatalysis is imperative for current environmental issues [5, 6] and energy problems [7, 8]. Anatase TiO₂ NPs (well-known ultraviolet (UV)-driven photocatalysts) are activated only by UV light (5% of the full solar spectrum) because of the high band gap of TiO₂ nanocrystals (anatase, ~3.2 eV) [9–11]; however, β-FeOOH (akaganeite, a photo-Fenton catalyst) triggers photocatalytic activity using visible light (~46% of the full solar spectrum) because of its narrow band gap (2.12 eV) [12, 13]. β-FeOOH photocatalysts have been utilized in the form of heterogeneous suspensions in contaminated water, which requires their recovery after each photocatalytic event [14, 15]. Immobilization of catalysts on the porous polymer platforms (membrane, mesh, cloth, etc.) has been demonstrated to overcome the limitation for β-FeOOH photocatalysts; a high photodegradation efficiency of ~100% for organic dyes under visible light and preservation of the photocatalytic activity above 90% after five cycles has been shown [12]. The easy recovery and cycling of nanocatalysts can be simply attempted by molecularly linking the active nanocatalysts with magnetic NPs, such as Fe₃O₄ NPs [16]. However, a complicated multi-step synthesis using sophisticated organic chemistry was needed to molecularly link the different nanomaterials in the previous reports. The strategy of mussel-inspired linking can be very effective to unlock this limitation and to provide a simple and fast platform for molecular linking between two different nanomaterials because dopamine- or polydopamine-mediated molecular linking is widely acceptable for various material platforms (substrates or particles) regardless of the chemical compositions and physical structures of platforms [3].

In this study, a β-FeOOH/Fe₃O₄ hybrid photocatalyst as a magnetically recyclable visible-driven hybrid photocatalyst is simply prepared by the incorporation of catechol-grafted polymers on the surface of Fe₃O₄ NPs and the subsequent growth of β-

FeOOH nanoneedles on the surface of catechol-modified Fe₃O₄ NPs. In addition to the role of molecular linking, the polycatecholic layers could be helpful in enhancing the photocatalytic activity of attached β-FeOOH photocatalysts through the action of the polycatecholic layers as an electron sink or acceptor, which minimizes the electron–hole recombination during visible-light-driven photocatalysis. Therefore, a β-FeOOH/Fe₃O₄ hybrid photocatalyst with an excellent visible-light-driven photodegradation efficiency toward organic dyes in wastewater through a photo-Fenton reaction in the presence of H₂O₂ and easy recovery/recycling performance with the help of external magnet can be simply prepared by the molecular linking strategy based on mussel-inspired chemistry of catecholic compounds.

Materials and methods

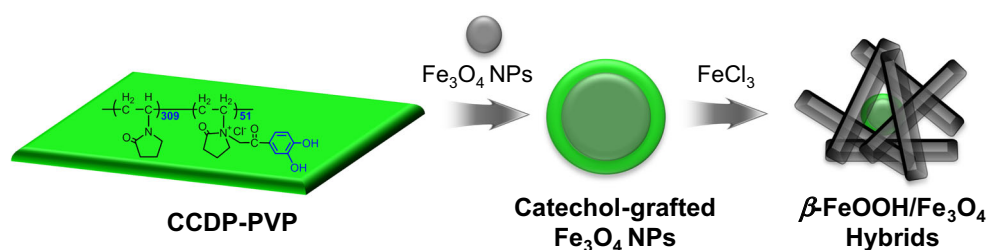
Materials and instruments

Poly(vinyl pyrrolidone) (PVP, MW = 40 000 Da), 2-chloro-3'-4'-dihydroxyacetophenone (CCDP), Fe₃O₄ NPs (50–100 nm, surface area > 60 m² g⁻¹), FeCl₃·6H₂O, tetrahydrofuran, hydrochloric acid (35–37%), ethanol, hexane, and hydrogen peroxide (30 wt%) were purchased from Sigma-Aldrich and used without further purification. Fourier transform infrared (FT-IR) spectra were acquired on a Nicolet iS10 FT-IR spectrometer (Thermo Scientific). Ultraviolet–visible (UV–Vis) spectra were recorded using an Optizen 2020UV spectrometer (Mecasys, South Korea). Field-effect scanning electron microscopy (FE-SEM) analysis was performed using a JSM-6700 microscope (JEOL, Japan), and the samples were prepared as powders. X-ray diffraction (XRD) measurements of the powder samples were recorded on a D8-Advance X-ray powder diffractometer (Bruker) using Cu Kα radiation (λ = 1.5406 Å). X-ray photoelectron spectroscopy (XPS) was performed using a Scientific Sigma Probe spectrometer (Thermo VG). The UV–Vis diffuse-reflectance spectroscopy (DRS) measurements were taken using a Lambda 750 spectrometer (Perkin Elmer) with BaSO₄ as a reference.

Synthesis of CCDP-PVP

The synthesis of catechol-grafted PVP (CCDP-PVP) was performed according to a previous report [17].

Figure 1 Schematic illustration for the preparation of the visible-light-driven β -FeOOH/Fe₃O₄ hybrid photocatalyst.



PVP (4.00 g) and CCDP (2.24 g) were dissolved in 50 mL of ethanol in a 100-mL flask. The mixture was then stirred at 70–80 °C for 24 h. After the reaction, 80% of the residual solvent was evaporated using a rotary evaporator, and the brownish white precipitate was isolated after precipitation into cold diethyl ether and subsequent vacuum filtration. A brown CCDP-PVP powder (4.03 g) was obtained after vacuum drying the precipitate at 30 °C for 12 h.

Synthesis of CCDP-PVP-grafted Fe₃O₄ NPs

CCDP-PVP (250 mg) was dissolved in 250 mL of ethanol at room temperature (25 °C). Then, Fe₃O₄ NPs (50 mg) were dispersed into 5 mL of tetrahydrofuran, and this dispersion was added dropwise into the above ethanol solution of CCDP-PVP. Then, the mixture was stirred for 24 h at room temperature. Finally, the solvent was removed using a rotary evaporator, and the resulting black powder was isolated by vacuum filtration and subsequent washing with diethyl ether. The CCDP-PVP-grafted Fe₃O₄ NPs (69 mg) were obtained after vacuum drying the powder at 30 °C for 12 h.

Synthesis of the β -FeOOH/Fe₃O₄ hybrid photocatalyst

A 0.067-M solution of FeCl₃·6H₂O was prepared in 20 mL of deionized water and 10 mL of a 0.01-M hydrochloric acid solution. Then, 50 mg of CCDP-PVP-grafted Fe₃O₄ NPs was added into the solution, and the reaction mixture was stirred at 60 °C for 24 h. After cooling to room temperature, the black powder was isolated by vacuum filtration and washing with deionized water. The β -FeOOH/Fe₃O₄ hybrid (38 mg) was obtained after vacuum drying the powder at 30 °C for 12 h.

Photocatalysis measurements

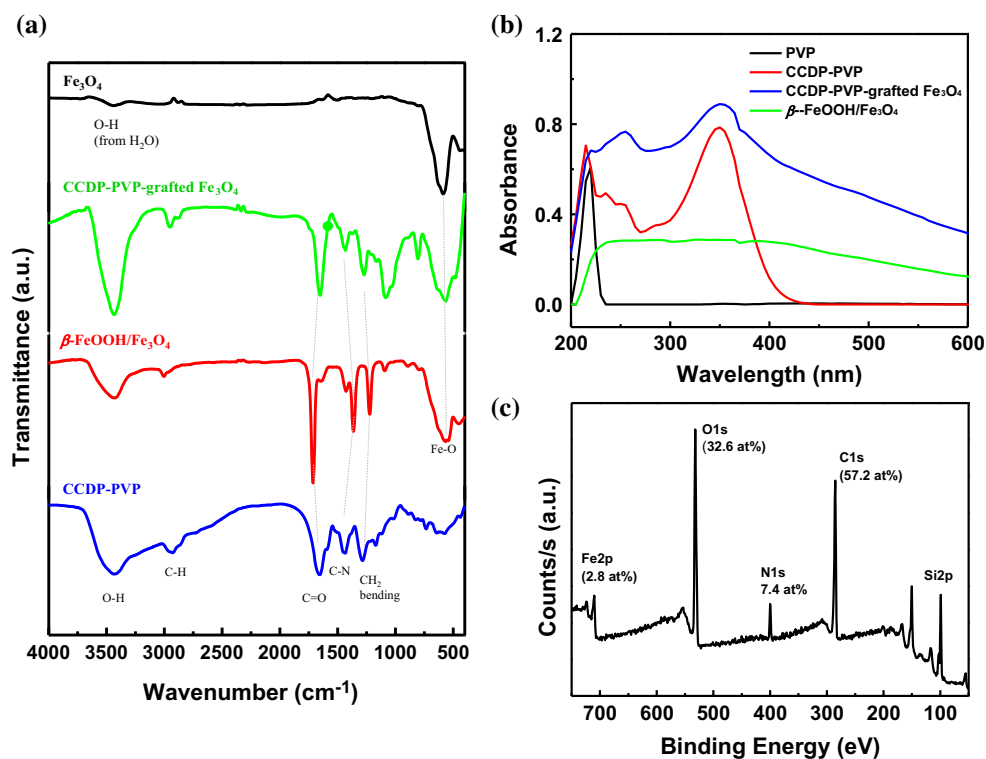
The photocatalytic activity of the β -FeOOH/Fe₃O₄ hybrid photocatalyst was evaluated by degrading rhodamine B under visible light generated by a 20-W halogen lamp (Osram) with a built-in UV cutoff filter of $\lambda > 400$ nm. The hybridized β -FeOOH/Fe₃O₄ photocatalyst (20 mg) was mixed with a 10-mL aqueous rhodamine B solution (10 mg L⁻¹) in the presence or absence of H₂O₂ at acidic condition (pH 2). Before evaluating the photocatalytic activity, the suspension was magnetically stirred in the dark for 30 min to reach an adsorption–desorption equilibrium. Then, the concentration of rhodamine B every 30 min of visible-light irradiation was determined from the absorption values at 560 nm measured by UV–Vis spectroscopy. The recovery and recycling of the β -FeOOH/Fe₃O₄ photocatalyst were attempted using an external magnet. After collection, the hybrid photocatalyst was briefly washed with continuous flushing of deionized water and tested immediately in another cycle of the photodegradation experiment without any drying.

Results and discussion

Preparation of the β -FeOOH/Fe₃O₄ hybrid photocatalyst

Catechol-grafted polymers play the key role as molecular glue or double-sided molecular adhesive between the β -FeOOH nanoneedles and Fe₃O₄ NPs (Fig. 1). As a catechol-grafted polymer, catechol-quaternized PVP was synthesized from the quaternization of CCDP with PVP (40,000 Da), producing CCDP-PVP with a high mass yield of 64% [18]. The number of catechol groups per single PVP chain is confirmed as 72 using ¹H-NMR spectroscopy, as previously reported [17].

Figure 2 a FT-IR spectrum, b XPS survey scan of CCDP-PVP-grafted Fe_3O_4 NPs, and c UV–visible spectrum of PVP, CCDP-PVP, CCDP-PVP-grafted Fe_3O_4 , and β - $\text{FeOOH}/\text{Fe}_3\text{O}_4$.



Grafting of CCDP-PVP on Fe_3O_4 NPs was performed in aqueous media. Catecholic compounds, such as dopamine or other catechol-rich polymers, can spontaneously bind onto the surface of various metal oxides by chelating of catechol moieties or ligand-to-metal charge transfer on metal oxides [19]. Facile grafting of CCDP-PVP on the surface of the Fe_3O_4 NPs is confirmed by the comparison of the FT-IR spectra of bare Fe_3O_4 NPs and CCDP-PVP-grafted Fe_3O_4 NPs (Fig. 2a). While bare Fe_3O_4 NPs reveal only a Fe–O stretching vibration at 590 cm^{-1} [20], CCDP-PVP-grafted Fe_3O_4 NPs showed additional

peaks at 1086 cm^{-1} (C–O stretching), 1272 cm^{-1} (C–N stretching), 1436 cm^{-1} (CH_2 bending), 1654 cm^{-1} (C=O stretching), 2953 cm^{-1} (C–H stretching), and 3430 cm^{-1} (O–H stretching), which are the characteristic peaks of CCDP-PVP [21], in addition to a peak at 566 cm^{-1} (F–O stretching). A XPS survey scan of CCDP-PVP-grafted Fe_3O_4 NPs clearly revealed the presence of N1s binding peaks at 402.2 eV with an abundance of 7.4 at% (Fig. 2b). With the incorporation of the catecholic layer, the UV–Vis spectrum of CCDP-PVP-grafted Fe_3O_4 NPs presented two characteristic optical absorption peaks at 255 and 360 nm that the peak at 225 nm originated

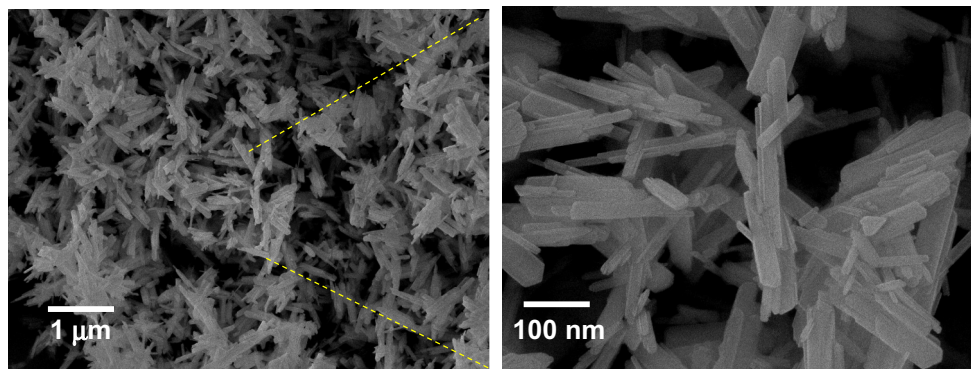
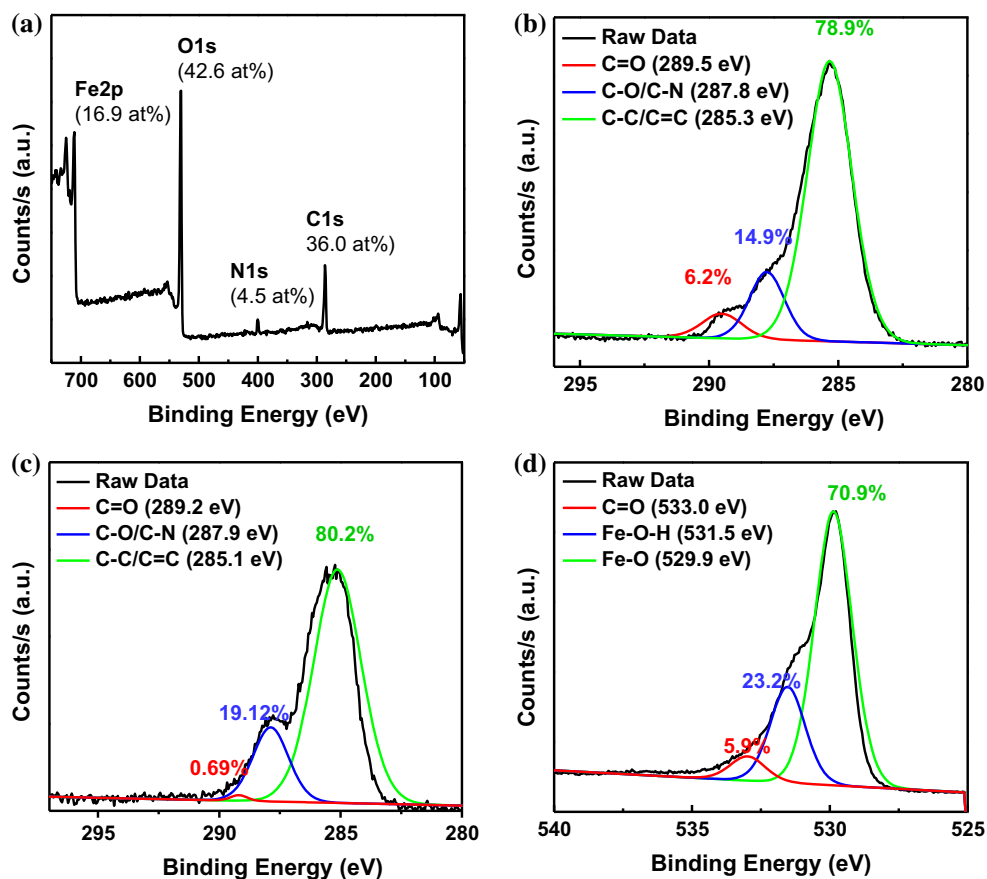


Figure 3 FE-SEM images of the β - $\text{FeOOH}/\text{Fe}_3\text{O}_4$ hybrid photocatalyst.

Figure 4 **a** XPS full survey scans of β -FeOOH/Fe₃O₄ hybrid photocatalyst, **b** C1 s high-resolution XPS spectra of CCDP-PVP-grafted Fe₃O₄, **c** C1 s, and **d** O1 s high-resolution XPS spectra of the β -FeOOH/Fe₃O₄ hybrid photocatalyst.



from the $n-\pi^*$ transition and that at 360 nm originated from the $\pi-\pi^*$ of the acetophenone structure of CCDP (Fig. 2c) [17]. The presence of C=O near the catechol group can partially extend the $\pi-\pi$ conjugation of the benzene groups, which results in a redshift of the $\pi-\pi^*$ transition from the typical value of 280 nm to 360 nm [22]. From all of these considerations, mussel-inspired grafting of CCDP-PVP on the surface of Fe₃O₄ NPs is clearly facile using our approach. In addition, the presence of free catecholic OH groups in CCDP-PVP-grafted Fe₃O₄ NPs is very interesting. Several non-chelated “free” catecholic moieties might still be present in addition to the PVP chains because a polycatecholic polymer was used instead of small catechol compounds, such as dopamine. While the degree of grafting of catecholic moieties of CCDP-PVP on the Fe₃O₄ NPs is not clear at this stage, it is highly promising that CCDP-PVP is anchored onto the Fe₃O₄ NPs and provides another “free” (non-anchored) catecholic moiety toward further decoration or molecular linking with other nanomaterials, such as β -FeOOH, as an efficient visible-light-driven photocatalyst.

Next, β -FeOOH nanorods were decorated onto CCDP-PVP-grafted Fe₃O₄ NPs by acid hydrolysis from FeCl₃, producing β -FeOOH/Fe₃O₄ hybrid nanomaterials. The growth of β -FeOOH nanorods on the CCDP-PVP-grafted Fe₃O₄ NPs was clearly identified from the FE-SEM image of the hybrids (Fig. 3). The length and width of the β -FeOOH nanorods are less than 1 μ m and 100 nm, respectively, and the Fe₃O₄ NPs were not visible because of the significant clustering of β -FeOOH nanorods after the hybridization process.

Characterization of the hybridized β -FeOOH/Fe₃O₄ photocatalyst

The FT-IR spectrum of the β -FeOOH/Fe₃O₄ hybrid nanomaterials showed a broad O–H stretching peak for the β -FeOOH or catecholic moieties at 3438 cm⁻¹, C=O stretching at 1714 cm⁻¹, and C–N stretching or CH₂ bending peaks at 1364 and 1221 cm⁻¹ (Fig. 2a). Interestingly, the C=O and C–N stretching peaks were significantly shifted to higher (+60 cm⁻¹ shift) and lower (–51 cm⁻¹ shift) wave numbers,

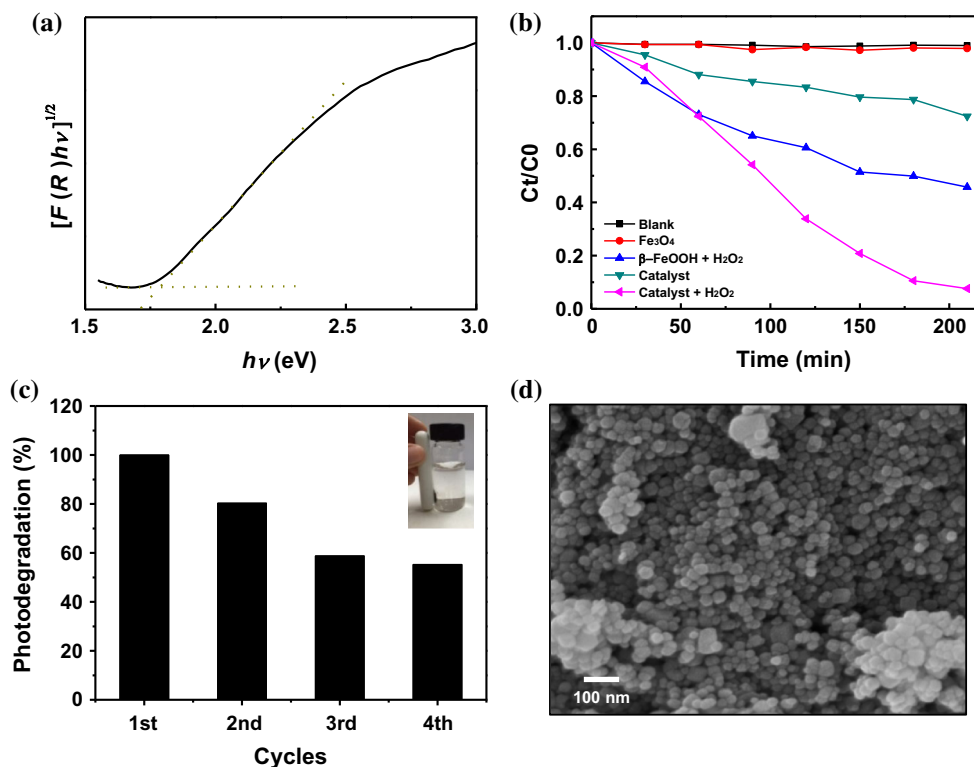


Figure 5 **a** UV-Vis-near IR reflectance spectrum of the β -FeOOH/ Fe_3O_4 hybrid photocatalyst, **b** photocatalytic degradation performance of rhodamine B under visible-light irradiation, **c** cycled visible-light photodegradation tests of rhodamine B

respectively, showing the dramatic change in the microenvironment around the catecholic layer of the CCDP-PVP-grafted Fe_3O_4 NPs after the incorporation of the β -FeOOH nanorods. A strong Fe–O stretching peak originating from both the Fe_3O_4 NPs and β -FeOOH nanorods is also observable at 580 cm^{-1} in the FT-IR spectra of the β -FeOOH/ Fe_3O_4 hybrid nanomaterials. The UV-Vis spectrum of the β -FeOOH/ Fe_3O_4 hybrid nanomaterials showed a broad absorption between 240 and 400 nm (Fig. 2c). This broad absorption is regarded as the π - π^* transition of catechol moieties, as discussed above. This absorption is continuously tailing, even over 600 nm, which is estimated to originate from Mie scattering by the presence of β -FeOOH nanorods with lateral dimensions larger than 100 nm [13]. The mussel-inspired molecular linking between the Fe_3O_4 NPs and β -FeOOH nanorods is clearly visualized when the external magnet is located near the hybrid nanomaterials. From the aqueous dispersion of the β -FeOOH/ Fe_3O_4 hybrid nanomaterials, all of the hybrid nanomaterials are immediately attracted to

based on recycling the β -FeOOH/ Fe_3O_4 hybrid photocatalyst, and **d** FE-SEM image of the β -FeOOH/ Fe_3O_4 hybrid photocatalyst after the fourth cycle.

the external magnet and no isolated particles are observed within the dispersion. All of the above characterizations confirm that the β -FeOOH/ Fe_3O_4 hybrid nanomaterial is successfully synthesized through mussel-inspired molecular linking with the incorporation of an intermediate catecholic layer.

The chemical composition of the β -FeOOH/ Fe_3O_4 hybrid nanomaterials was carefully examined by XPS spectroscopy. An XPS full survey scan of the β -FeOOH/ Fe_3O_4 hybrid showed the presence of Fe, O, N, and C with abundances of 16.9, 42.6, 4.5, and 36.0 at%, respectively (Fig. 4a). For comparison, CCDP-PVP-grafted Fe_3O_4 NPs showed the presence of Fe, O, N, and C of 2.8, 32.6, 7.4, and 57.2 at%, respectively (Fig. 2b). The increased Fe content in the β -FeOOH/ Fe_3O_4 hybrid was expected and supports the growth and molecular linking of β -FeOOH on CCDP-PVP-grafted Fe_3O_4 NPs. Both C and N in the CCDP-PVP-grafted Fe_3O_4 NPs and β -FeOOH/ Fe_3O_4 hybrid nanomaterials originate from the catecholic layer present between the β -FeOOH nanorods and Fe_3O_4 NPs. Comparison of the high-resolution Fe2p, O1s,

C1 s, and N1 s binding peaks clearly showed the formation of β -FeOOH on the CCDP-PVP-grafted Fe_3O_4 NPs. The high-resolution C1 s binding peak of the CCDP-PVP-grafted Fe_3O_4 NPs showed the characteristic C–C/C=C, C–O/C–N, and C=O binding peaks at 285.3 eV (78.9%), 287.8 eV (14.9%), and 289.5 eV (6.2%), respectively, showing the formation of a polycatecholic layer on the surface of the Fe_3O_4 NPs through mussel-inspired grafting of CCDP-PVP (Fig. 4b) [23]. Interestingly, the above C=O binding peak is reduced in the high-resolution C1 s binding peak of the β -FeOOH/ Fe_3O_4 hybrid nanomaterials, which implies that the nucleation of β -FeOOH nanorods from Fe^{3+} ions might occur near the C=O bonds of pyrrolidone moieties of the catecholic layer (Fig. 4c). In addition, the high-resolution O1 s binding peak of the β -FeOOH/ Fe_3O_4 hybrid nanomaterials showed the presence of Fe–O–H binding at 531.5 eV, which again confirms the presence of β -FeOOH in the hybrid nanomaterials (Fig. 4d) [24]. High-resolution N1 s and Fe2p binding peaks of both the CCDP-PVP-grafted Fe_3O_4 NPs and β -FeOOH/ Fe_3O_4 hybrid nanomaterials did not show any noticeable differences, revealing N1 s binding peak at 400 eV and Fe2p binding peaks at 724.3 and 710.2 eV ($\text{Fe}2p_{1/2}$ and $\text{Fe}2p_{3/2}$) (Figure S1) [12]. The morphology of grown β -FeOOH on the surface of the β -FeOOH/ Fe_3O_4 hybrid nanomaterials was measured by XRD, and the characteristic scattering peaks of β -FeOOH were identified together with the characteristic peaks of the Fe_3O_4 NPs (Figure S2). Therefore, all of these characterizations clearly support the successful synthesis of the β -FeOOH/ Fe_3O_4 hybrid nanomaterials through molecular linking by the catechol-grafted polymer.

Visible-light-driven photodegradation of rhodamine B by the β -FeOOH/ Fe_3O_4 hybrid photocatalyst

The optical band gap of the prepared β -FeOOH/ Fe_3O_4 hybrid nanomaterials was measured as 1.79 eV (corresponding to 693 nm) from the UV–Vis DRS spectrum of the hybrid photocatalysts (Fig. 5a). Considering that the optical band gap of β -FeOOH itself is 2.12 eV [25], significant band gap narrowing occurred in the β -FeOOH/ Fe_3O_4 hybrid nanomaterials, probably because of the buildup of intermediate energy levels incorporated from the nearby catecholic

layer [26]. Therefore, the β -FeOOH/ Fe_3O_4 hybrid nanomaterial photocatalysts can absorb most visible-light wavelengths up to 690 nm in addition to UV light, and the photocatalysis of the hybrid photocatalyst can be triggered by visible light.

The photocatalytic activity of the β -FeOOH and the β -FeOOH/ Fe_3O_4 nanomaterials was evaluated by monitoring the optical absorption of rhodamine B as a model dye in wastewater under visible-light irradiation from a lamp with or without H_2O_2 . Photodegradation of the aqueous rhodamine B solution (pH 2) by the β -FeOOH/ Fe_3O_4 hybrid photocatalysts was almost complete (92%) within 3 h of visible-light irradiation in the presence of H_2O_2 , deliberating the photodegradation of the rhodamine B by the β -FeOOH itself is just 65%, which is an indispensable agent for photo-Fenton photocatalysis (Fig. 5b). In this photo-Fenton reaction, pH value also takes effect in the photodegradation of rhodamine B because abundant $\text{OH}\cdot$ are produced at the acidic condition [12]. At pH 3 and 5, above photodegradation was dramatically deactivated and only photodegradation less than 20% was enabled in the same condition (Figure S3).

The photocatalytic performances of the hybrid photocatalysts were also measured under UV light (365 nm). Within 90 min of UV irradiation, 75% of rhodamine B was decomposed (Figure S4). In both cases, the catalytic activities of the hybrid catalysts were enhanced in the presence of H_2O_2 . This enhanced photodegradation efficiency observed for the β -FeOOH/ Fe_3O_4 hybrid photocatalyst can be attributed to the heterogeneous photo-Fenton-like process, where plentiful free hydroxyl radicals are promptly generated from the reaction between β -FeOOH and H_2O_2 under UV or Vis irradiation [27]. The catecholic layer not only links the β -FeOOH nanorods and Fe_3O_4 NPs, but also enhances the photocatalytic activity of the β -FeOOH photocatalyst. In addition to the band gap narrowing of the semiconductor, the electron accepting catecholic layers can gather photo-generated electrons from the conduction band of the β -FeOOH nanorods. The remaining holes on the valence band of the β -FeOOH nanorods can generate $\text{OH}\cdot$, which is highly reactive for the decomposition of organic pollutants, such as rhodamine B. Therefore, the β -FeOOH/ Fe_3O_4 hybrid photocatalyst demonstrates an enhanced photocatalytic activity because of the presence of the catecholic layer.

The β -FeOOH/Fe₃O₄ hybrid photocatalysts can be repeatedly isolated and recycled with the help of an external magnet because of the presence of magnetically responsive Fe₃O₄ NPs in the hybrid photocatalysts (Movie S1). The photodegradation efficiency of the hybrid photocatalysts for rhodamine B continuously decreases with recycling, and it finally saturates at a value of 55% after the fourth cycle (Fig. 5c). The reduced photocatalytic activity of the β -FeOOH/Fe₃O₄ hybrid photocatalysts upon recycling likely originates from the morphological change in the photocatalysts. An FE-SEM image of the photocatalyst after the fourth cycle showed a dot-like morphology rather than the pristine rod-like morphology (Fig. 5d). Surface poisoning of the photocatalysts by various intermediate compounds during the photodegradation might additionally contribute to lower the photocatalytic activity after prolonged recycling [28, 29]. To accomplish a similar photodegradation efficiency, much longer reaction times (greater than 12 h) were required upon irradiation of visible light.

Conclusion

In conclusion, the molecular linking strategy was successfully performed for the synthesis of the β -FeOOH/Fe₃O₄ hybrid photocatalysts as visible-light-driven photocatalysts. In addition to the linking of magnetic Fe₃O₄ NPs with β -FeOOH nanoneedles, the presence of the catecholic layer near β -FeOOH accelerates the photocatalysis by either band gap narrowing or electron accepting ability. The β -FeOOH/Fe₃O₄ hybrid photocatalysts showed a high photocatalytic degradation efficiency for rhodamine B as a model compound for environmental pollutants under UV or even visible-light illumination. The presence of magnetic Fe₃O₄ NPs enabled simple recovery and recycling of the hybrid photocatalysts using an external magnet. Catechol-mediated molecular linking can provide a wide range of hybrid nanomaterials. While the number of β -FeOOH nanoneedles in the single β -FeOOH/Fe₃O₄ hybrid is not clear in this study, we believe that AB_x-type hierarchical hybrid structures could be prepared by this approach, where A and B are two different nanomaterials with completely different compositions and morphologies.

Acknowledgements

This research was supported by Basic Science Research Program through the National Research Foundation of Korea (NRF) funded by the Ministry of Education (2015R1D1A3A01020192) and a Grant (No. 10049064) by Industrial Technology Innovation Program funded by Ministry of Trade, Industry & Energy (MI, Korea).

Compliance with ethical standards

Conflicts of interest The authors declare that there are no conflicts of interest related to the publication of this paper.

Electronic supplementary material: The online version of this article (doi:[10.1007/s10853-017-0910-3](https://doi.org/10.1007/s10853-017-0910-3)) contains supplementary material, which is available to authorized users.

References

- [1] Kim SY, Lee MY, Lee JY, Park YH, Kim HG, Jeong CJ, Mosaibab T, Park B, Park SY, In I (2013) Mussel-inspired engineering of an anodized aluminum oxide membrane. *Chem Lett* 42:902–903
- [2] Park YH, Jeong CJ, Park CP, Park SY, In I (2014) Photoresponsive modulation of mass transfer through spiropyran-grafted anodized aluminum oxide membrane. *Chem Lett* 43:1540–1541
- [3] Liu Y, Ai K, Lu L (2014) Polydopamine and its derivative materials: synthesis and promising application in energy, environmental, and biomedical fields. *Chem Rev* 114:5057–5115
- [4] Jo S, Park YH, Ha SG, Kim SM, Song C, Park SY, In I (2015) Simple noncovalent hybridization of polyaniline with graphene and its application for pseudocapacitor. *Synth Met* 209:60–67
- [5] Morales-Torres S, Pastrana-Martínez LM, Figueiredo JL, Faria JL, Silva AMT (2012) Design of graphene-based TiO₂ photocatalyst—a review. *Environ Sci Pollut Res* 19:3676–3687
- [6] Daghrir R, Drogui P, Robert D (2013) Modified TiO₂ for environmental photocatalytic applications: a review. *Ind Eng Chem Res* 52:3581–3599
- [7] Hamdy MS, Amrollahi R, Sinev I, Mei B, Mul G (2014) Strategies to design efficient silica-supported photocatalyst for reduction CO₂. *J Am Chem Soc* 136:594–597

- [8] Meijnenburg AW, Veerbeek J, de Putter R, Veldhuis SA, Zootjes MGC, Mul G, Mntero-Moreno JM, Nielsch K, Schäfer H, Steinhart M, ten Elshof JE (2014) Electrochemical synthesis of coaxial TiO₂-Ag nanowires and their application in photocatalytic water splitting. *J Mater Chem A* 2:2648–2656
- [9] Chen X, Liu L, Yu PY, Mao SS (2011) Increasing solar absorption for photocatalysis with black hydrogenated titanium dioxide nanocrystals. *Science* 311:746–750
- [10] Lang X, Ma W, Chen C, Ji H, Zhao J (2014) Selective aerobic oxidation mediated by TiO₂ photocatalysis. *Acc Chem Res* 47:355–363
- [11] Liu K, Cao M, Fujishima A, Jiang L (2014) Bio-inspired titanium dioxide materials with special wettability and their applications. *Chem Rev* 114:10044–10094
- [12] Zhang C, Yang H-C, Wan L-S, Liang H-Q, Li H, Xu Z-K (2015) Polydopamine-coated porous substrates as a platform for mineralized & #x03B2;-FeOOH nanorods with photocatalysis under sunlight. *ACS Appl Mater Interfaces* 7:11567–11574
- [13] Zhu T, Ong WL, Zhu L, Ho GW (2015) TiO₂ fibers supported & #x03B2;-FeOOH nanostructures as efficient visible light photocatalyst and room temperature sensor. *Sci Rep* 5:10601
- [14] Benz M, van der Kraan AM, Prins R (1998) Reduction of aromatic nitrocompounds with hydrazine hydrate in the presence of an iron oxide hydroxide catalyst—II. Activity, X-ray diffraction and Mossbauer study of the iron oxide hydroxide catalyst. *Appl Catal A* 172:149–157
- [15] Yuan Z-Y, Ren T-Z, Su B-L (2004) Surfactant mediated nanoparticle assembly of catalytic mesoporous crystalline iron oxide materials. *Catal Today* 93–95:743–750
- [16] Geng Z, Lin Y, Yu X, Shen Q, Ma L, Li Z, Pan N, Wang X (2012) Highly efficient dye adsorption and removal: a functional hybrid of reduced graphene oxide-Fe₃O₄ nanoparticles as an easily regenerative adsorbent. *J Mater Chem* 22:3527–3535
- [17] Mosaiab T, Jeong CJ, Shin GJ, Choi KH, Lee SK, Lee I, In I, Park SY (2013) Recyclable and stable silver deposited magnetic nanoparticles with poly(vinyl pyrrolidone)-catechol coated iron oxide for antimicrobial activity. *Mater Sci Eng, C* 33:3786–3794
- [18] Kim SM, Park YH, Seo SW, Park CP, Park SY, In I (2015) Mussel-inspired immobilization of catalyst for microchemical application. *Adv Mater Interfaces* 2:1500174–1500179
- [19] Tang W, Policastro GM, Hua G, Gou K, Zhou J, Wesdemiotis C, Doll GL, Becker ML (2014) Bioactive surface modification of metal oxides via catechol-bearing modular peptides: multivalent-binding, surface retention, and peptide bioactivity. *J Am Chem Soc* 136:16357–16367
- [20] Asgari S, Fakhari Z, Berijani S (2014) synthesis and characterization of Fe₃O₄ magnetic nanoparticles coated with carboxymethyl chitosan grafted sodium methacrylate. *J Nanostruct* 4:55–63
- [21] Jiang J, Zhu L, Zhu L, Zhang H, Zhu B, Xu Y (2013) Antifouling and antimicrobial polymer membranes based on bioinspired polydopamine and strong hydrogen-bonded poly(*N*-vinyl pyrrolidone). *ACS Appl Mater Interfaces* 5:12895–12904
- [22] Sever MJ, Wilker JJ (2004) Visible absorption spectra of metal-catecholate and metal-tironate complexes. *Dalton Trans* 7:1061–1072
- [23] Kang SM, Park S, Kim D, Park SY, Rouff RS, Lee H (2011) Simultaneous reduction and surface functionalization of graphene oxide by mussel-inspired chemistry. *Adv Funct Mater* 21:108–111
- [24] Martinez L, Leinen D, Martin F, Gabas M, Ramos-Barrado RJR, Quagliata E, Dalchiele EA (2007) Electrochemical growth of diverse iron oxide (Fe₃O₄, & #x03B1;-FeOOH. And & #x03B3;-FeOOH) thin films by electrodeposition potential tuning. *J Electrochem Soc* 154:D126–D133
- [25] Chowdhury M, Ntribinyange M, Nyamayaro K, Fester V (2015) Photocatalytic activities of ultra-small & #x03B2;-FeOOH and TiO₂ heterojunction structure under simulated solar irradiation. *Mater Res Bull* 68:133–141
- [26] Stahk HG, Hogan PA, Schmidt WL, Wall SJ, Buhrlage A, Bullen HA (2010) Surface complexation of catechol to metal oxides: an ATR-FTIR, adsorption, and dissolution study. *Environ Sci Technol* 44:4116–4121
- [27] Wang C, Liu H, Sun Z (2012) Heterogeneous photo-Fenton reaction catalyzed by nanosized iron oxide for water treatment. *Int J Photoenergy* 2012:121239–121249
- [28] Li L, Chen R, Zhu X, Wang H, Wang Y, Liao Q, Wang D (2013) Optofluidic microreactors with TiO₂-coated fiber-glass. *ACS Appl Mater Interfaces* 5:12548–12553
- [29] Krivec M, Dillerr R, Bahnemann DW, Mehle A, Strancar J, Drazic G (2014) The nature of chlorine-inhibition of photocatalytic degradation of dichloroacetic acid in a TiO₂-based microreactor. *Phys Chem Chem Phys* 16:14867–14873